ACS NANO

www.acsnano.org

ARTICLE

Enhanced Photodetection Performance of an In Situ Core/Shell Perovskite-MoS_2 Phototransistor

Jinwoo Sim,◆ Sunggyu Ryoo,◆ Joo Sung Kim,◆ Juntae Jang, Heebeom Ahn, Donguk Kim, Joonha Jung, Taehyun Kong, Hyeonmin Choi, Yun Seog Lee, Tae-Woo Lee,* Kyungjune Cho,* Keehoon Kang,* and Takhee Lee*

Cite This: *ACS Nano* 2024, 18, 16905−16913

Read Online

ACCESS | Metrics & More | Article Recommendations | Supporting Information

ABSTRACT: **While two-dimensional transition metal dichalcogenides (TMDCs)-based photodetectors offer prospects for high integration density and flexibility, their thinness poses a challenge regarding low light absorption, impacting photodetection sensitivity. Although the integration of TMDCs with metal halide perovskite nanocrystals (PNCs) has been known to be promising for photodetection with a high absorption coefficient of PNCs, the low charge mobility of PNCs delays efficient photocarrier injection into TMDCs. In this study, we integrated MoS_2 with in situ formed core/shell PNCs with short ligands that minimize surface defects and enhance photocarrier injection. The PNCs/MoS_2 heterostructure efficiently separates electrons and holes by establishing type II band alignment and consequently inducing a photogating effect. The synergistic interplay between photoconductive and photogating effects yields a high responsivity of 2.2×10^6 A/W and a specific detectivity of 9.0×10^{11} Jones. Our findings offer a promising pathway for developing low-cost, high-performance phototransistors leveraging the advantages of two-dimensional (2D) materials.**

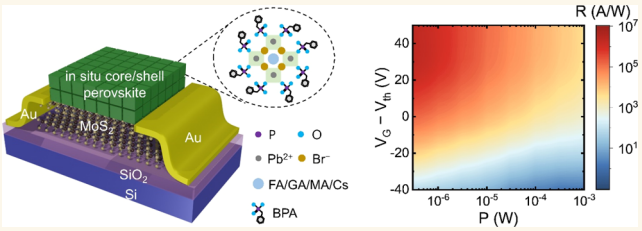

KEYWORDS: *heterostructure phototransistor, perovskite nanocrystal, transition metal dichalcogenide, photoconductive effect, photogating effect*

Two-dimensional (2D) transition metal dichalcogenides (TMDCs) are promising materials for use in a variety of optoelectronic device applications due to their tunable band gap, simple fabrication, intriguing excitonic properties, and high carrier mobility.[1−4] Therefore, there have been extensive efforts to exploit these outstanding properties of 2D TMDCs for optoelectronics, especially photodetectors.[5−10] Photodetectors are basic components of optoelectronics and have applications in various fields such as thermal imaging cameras, optical communications, machine vision technology, and more. However, 2D TMDCs have low light absorption due to their atomic-level thinness, posing a limitation for sensitive photodetection.[11]

To enhance the light absorption of atomically thin TMDCs, various strategies have been proposed, such as designing plasmonic structures,[12] fabricating in-plane p−n junctions through electrostatic gating,[13] modulating electronic structures through 2D/2D heterostructures,[14−17] and integrating highly optically absorbing materials.[18−21] Among these strategies, heterostructures incorporating lead halide perovskite materials known for their high optical efficiency, tunable band gap, and solution processability have received considerable attention.[18−20,22] In particular, recent studies have reported significant performance improvements using perovskite nanocrystals (PNCs), which are zero-dimensional (0D) structures of a perovskite. Light absorption can be maximized through the 0D structure of PNCs, but there is a trade-off of degraded carrier mobility and lower charge injection into TMDC layers, caused by the insulating organic ligands surrounding PNCs.[11,23,24]

To address the limitations of conventional PNCs and improve the performance of TMDC photodetectors, we integrated MoS_2 phototransistors with in situ formed core/

Received: February 28, 2024
Revised: May 27, 2024
Accepted: June 7, 2024
Published: June 21, 2024

https://doi.org/10.1021/acsnano.4c02775
ACS Nano 2024, 18, 16905−16913

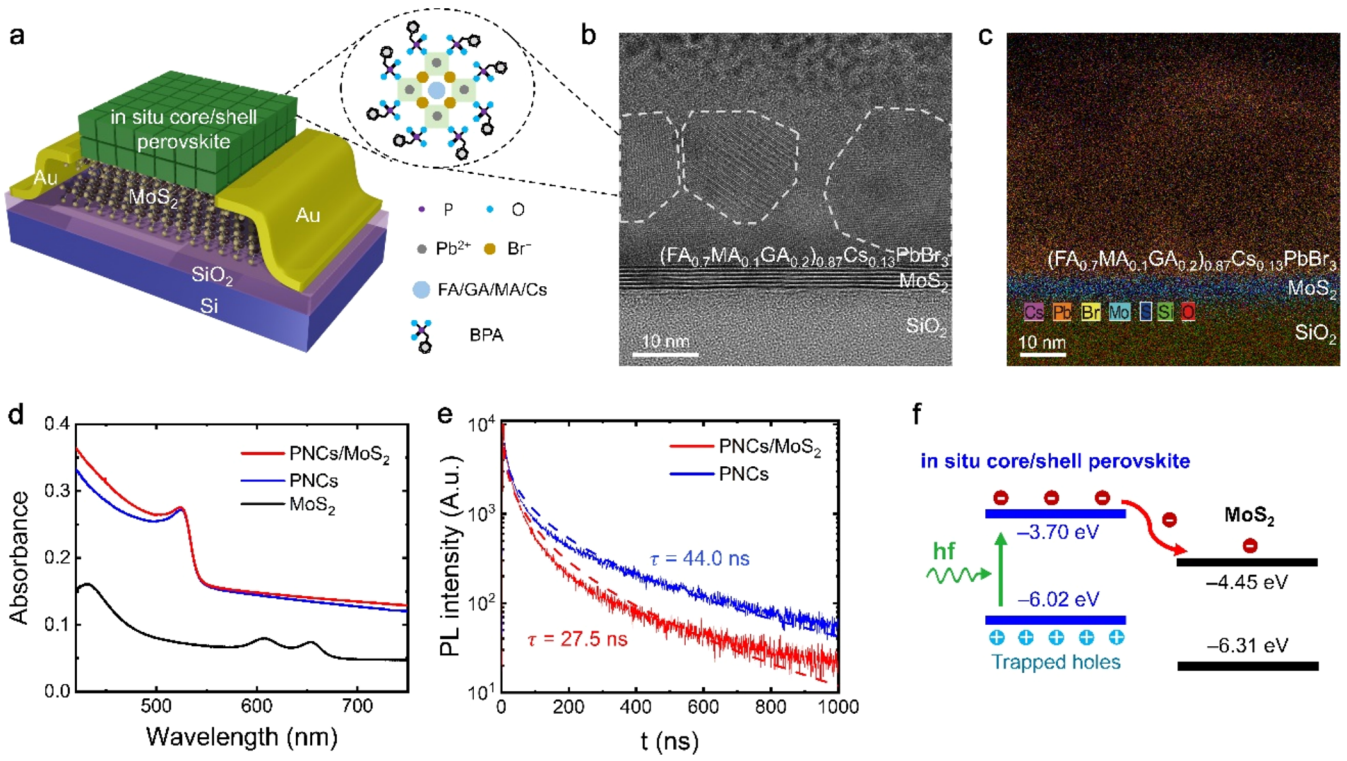

Figure 1. Characteristics of the device. (a) Schematic of PNCs/MoS_2 phototransistor. (b) Cross-sectional TEM image and (c) EDS mapping image of PNCs/MoS_2 phototransistor. (d) UV−vis absorption spectra image of the MoS_2, PNCs, and the PNCs/MoS_2 phototransistor. (e) TRPL image of the MoS_2 phototransistor before and after spin-coating the in situ core/shell perovskite. (f) Band alignment of PNCs/MoS_2 phototransistor.

shell PNCs. As some of us have previously reported,[24] in situ core/shell perovskites are created by splitting three-dimensional (3D) perovskite films using benzylphosphonic acid (BPA), which significantly reduces the size of the ligands and minimizes defects. This leads to enhanced carrier mobility of the PNCs and rapid charge injection into TMDC layers.[24] Due to these properties, our PNCs/MoS_2 phototransistors exhibited high values of photodetection figures of merit, i.e., a maximum responsivity of 2.2×10^6 A/W and a maximum specific detectivity of 9.0×10^{11} Jones, highlighting its enhanced performance as a phototransistor. We also investigated the photocurrent generation mechanisms of the PNCs/MoS_2 phototransistor, namely, photoconduction and photogating, and discovered their effects on photocurrent by manipulating the gate voltage, ultimately identifying the conditions that yield the best performance. Our research contributes to a deeper understanding of the photocurrent generation phenomena in TMDC phototransistors and offers a promising approach to the study of high-performance phototransistors based on 2D materials.

RESULTS AND DISCUSSION

The device schematic of the PNCs/MoS_2 phototransistor is shown in Figure 1a. In situ formed core/shell PNCs are integrated as a photosensitive layer on top of the MoS_2 field effect transistors (FETs). Details about the device fabrication can be found in the Supporting Information. We examined the PNCs/MoS_2 heterostructure through a transmission electron microscope (TEM) to verify that the PNCs layer is well synthesized on top of the MoS_2 layer. The cross-sectional TEM image of Figure 1b shows the core/shell structure of the PNCs with a cubic crystalline core with a lattice distance of ∼5.8 Å, identical to our previously reported PNCs synthesized on other substrates.[24] A clean interface between the PNCs and the MoS_2 layer was confirmed, which is crucial for the photodetection performance of the device. In addition, the energy-dispersive X-ray (EDS) mapping image of Figure 1c validates the chemical compositions of the PNCs and MoS_2 in the heterostructure. Note that the typical exciton diffusion length in PNCs exceeds several hundred nanometers,[25] and the thickness of the PNCs layer (∼60 nm, Figure S2) is suitable for excitons generated in the uppermost layer of the PNC to migrate to the PNCs/MoS_2 interface before recombination within the PNCs layer (Figure S3).

The role of PNCs as photosensitive layers is to efficiently absorb light and inject photogenerated carriers into the MoS_2 channel. We performed optical characterizations to confirm that the PNCs layer is effective as a photosensitive layer, as shown in Figure 1d,e. First, the ultraviolet−visible (UV−vis) spectra in Figure 1d demonstrate that the light absorption in the PNCs/MoS_2 heterostructure is significantly increased compared to that of MoS_2 alone. The enhancement of light absorption can be attributed to the high light absorption coefficient of lead halide perovskites.[22] Moreover, the absorbance spectra of the PNCs/MoS_2 heterostructure and isolated PNCs show similar intensities, indicating that the light absorption of the MoS_2 layer is negligible in the PNCs/MoS_2 heterostructure. It shows that lights will mainly be absorbed by the PNCs photosensitive layer in the PNCs/MoS_2 phototransistor. This can also be seen by comparing the absorbance peak after the integration of the PNCs layer on MoS_2. The absorption spectrum of the MoS_2 shows two excitonic peaks between 600 and 700 nm which originate from the A and B direct excitonic transitions, and another excitonic peak near

https://doi.org/10.1021/acsnano.4c02775
ACS Nano 2024, 18, 16905−16913

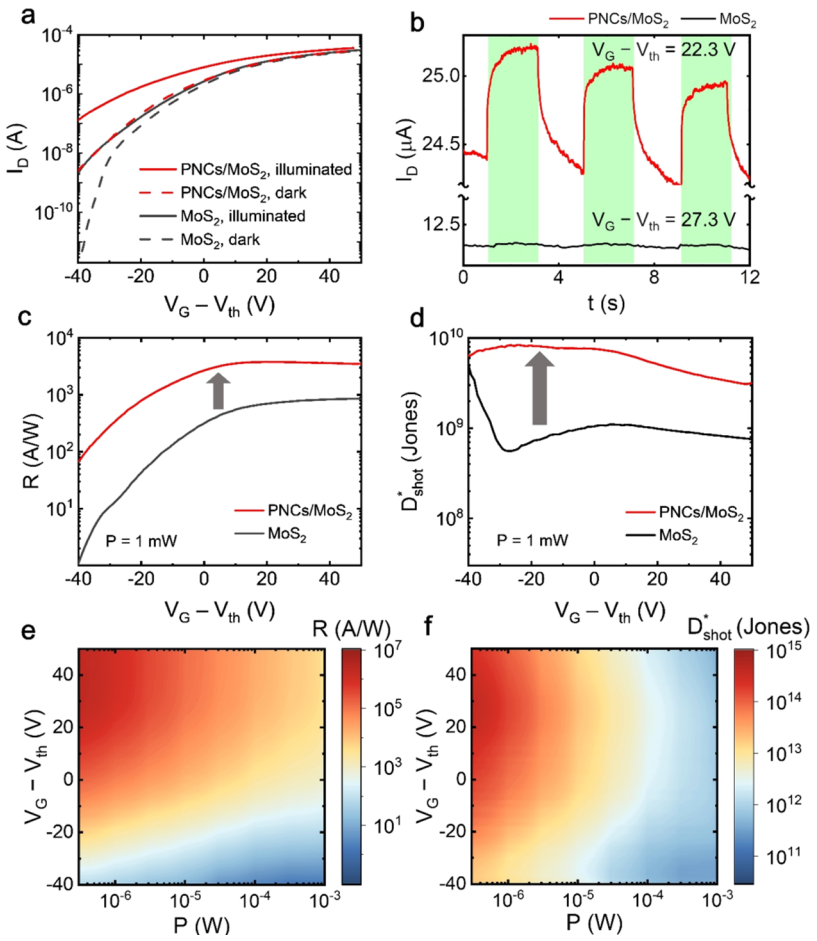

Figure 2. Optoelectrical properties of the device. (a) Transfer curves and (b) photoresponses of PNCs/MoS_2 and MoS_2 phototransistors at a laser power of 1 mW. (c) Responsivity and (d) specific detectivity derived from shot noise of PNCs/MoS_2 and MoS_2 phototransistors at a laser power of 1 mW. (e) Responsivity and (f) specific detectivity derived from shot noise of the PNCs/MoS_2 phototransistor in different gate voltage and laser power. All measurements were conducted at V_D = 0.1 V.

400 nm which is related to C-exciton.[26,27] On the other hand, the absorption spectrum of the PNCs/MoS_2 heterostructure lacks the excitonic peaks characteristic of MoS_2. Instead, an absorption peak at 540 nm appears, corresponding to the distinct band edge absorption peak of PNCs, as confirmed in our previous report.[24] This observation further confirms the dominant role of the PNCs layer in light absorption.

Time-resolved photoluminescence (TRPL) analysis was performed to verify that photogenerated electrons are transferred to the MoS_2 channel from the photosensitive layer (the PNCs) in Figure 1e. The PL intensity decay was fitted to the stretched exponential function $I(t) = I(0)\exp[-(t/\tau^*)^{\beta}]$. In this equation, β is the stretching parameter, and τ^* is the time constant. The stretched exponential function is commonly used to model the time relaxation behaviors in disordered systems, such as the TRPL decay.[28,29] The PL lifetime (τ value) can be obtained by the equation $\tau = \int_0^{\infty} \exp[-(t/\tau^*)^{\beta}]dt = \frac{\tau^*}{\beta}\Gamma\left(\frac{1}{\beta}\right)$, where Γ is the gamma function. The PL lifetime observed for the PNCs/MoS_2 heterostructure (~27.5 ns) is shorter compared to that of the PNCs (~44.0 ns), suggesting that radiative recombination decreased within the PNCs/MoS_2 heterostructure. This is attributed to the efficient charge transfer of photogenerated carriers from the PNCs to the MoS_2 layer.

Photogenerated carrier transfer from the PNCs to the MoS_2 can be explained by the type II band alignment of the PNCs/MoS_2 heterostructure as shown in Figure 1f. The band alignments are confirmed by Kelvin probe force microscopy and ultraviolet photoelectron spectroscopy (Figure S6).[30] When electron–hole pairs are generated within the PNCs, electrons from the PNCs tend to transfer to the MoS_2 due to the lower conduction band minimum level of the MoS_2 compared with that of PNCs. On the other hand, holes remain trapped within the PNCs, since the valence band of PNCs has a higher energy level than that of the MoS_2. Here, the rate of electron transfer (κ) can be calculated by the equation

$$\kappa = \frac{1}{\tau_{\mathrm{PNCs/MoS_2}}} - \frac{1}{\tau_{\mathrm{PNCs}}} \quad (1)$$

where $\tau_{\mathrm{PNCs/MoS_2}}$ and τ_{PNCs} are the PL lifetime of PNCs/MoS_2 heterostructure and PNCs layer, respectively.[23] In our study, κ was found to be ~10^7 s^{-1}, indicating the rapid transfer of photogenerated electrons from the PNCs to the MoS_2, compared to previously reported devices.[23,31] These charge transfer behaviors of the photogenerated electrons and holes result in both a photoconductive effect and a photogating effect. The photoconductive effect stems from the increased carrier density of the n-type MoS_2 channel due to the

https://doi.org/10.1021/acsnano.4c02775
ACS Nano 2024, 18, 16905–16913

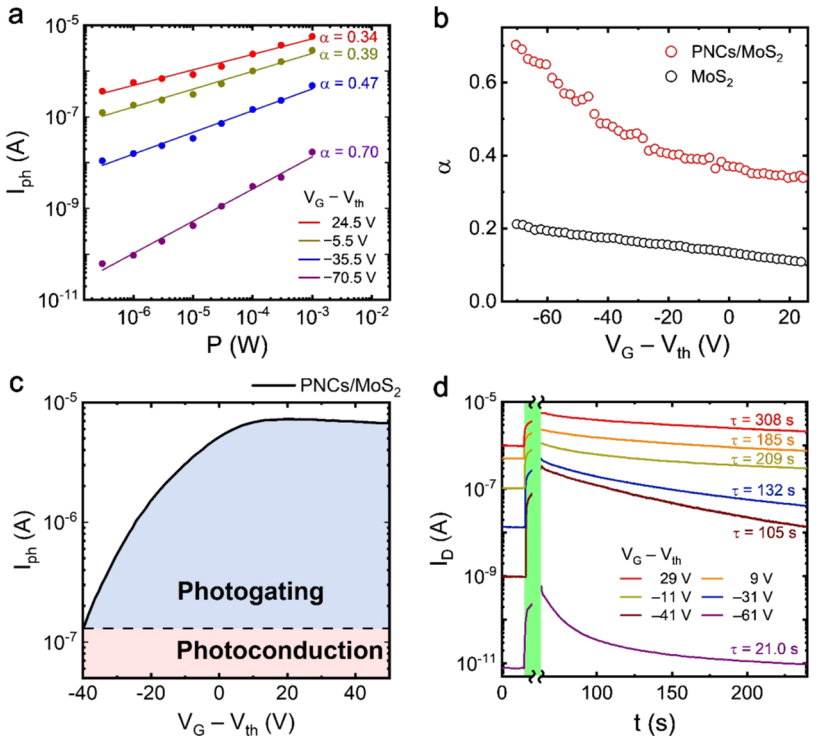

Figure 3. Photocurrent generation mechanisms of the PNCs/MoS_2 phototransistor. (a) The photocurrent curves fitted to a simple power law for laser power. (b) The gate voltage dependence of α. (c) Gate dependence of the photocurrent. (d) Response time of the device as a function of gate voltage.

transferred electrons. On the other hand, the photogating effect emerges through the accumulation of holes in the PNCs, leading to a positive gating effect that subsequently amplifies the photocurrent within the MoS_2 channel.[5]

To confirm the improvement of the photodetection performance due to the integration of the PNCs, we compared the optoelectronic properties of the PNCs/MoS_2 phototransistor with those of the MoS_2 phototransistor without the PNCs layer using a 532 nm laser with an optical power of 1 mW. Note that a moderate optical power of 1 mW was selected to maintain the stability of the phototransistor, preventing any potential damage due to excessively strong light illumination. The transfer characteristics, i.e., drain current (I_D) versus overdrive voltage ($V_G - V_{th}$, V_{th} is threshold voltage) of the devices are shown in Figure 2a. In this figure, the drain currents were plotted against the overdrive voltage to compare the currents at the same gate voltage above the threshold voltage. Here, the photocurrent (I_{ph}) is defined by the following equation $I_{ph} = I_{illum} - I_{dark}$, where I_{illum} and I_{dark} are each current under illuminated and dark conditions. As shown in Figure 2a, the PNCs/MoS_2 phototransistor exhibits higher I_{ph} and I_{illum} values compared to those of the MoS_2 phototransistor. This amplified photoresponse arises from the increased light absorption in the PNCs layer coupled with the synergistic interaction of the photoconductive and photogating effects due to the type II band alignment of the PNCs/MoS_2 heterostructure (Figure 1f). It should be noted that the increase in dark current at low gate voltage, reaching near a nanoampere, is attributed to electron transfer due to the energy level difference between the PNCs and MoS_2, as well as a leakage current of 0.2 nA through the PNCs layer (Figure S8). However, in most gate regions, the leakage current through the PNCs is negligible compared to the photocurrent in the range of several μA, and it does not affect the operation mechanism and the performance of the device.

Enhanced photoresponse of the PNCs/MoS_2 phototransistor is more distinctly evident in the dynamic photoswitching behavior in Figure 2b. A light pulse with a duration of 2 s was applied every 4 s to compare the photoswitching behavior at the similar value of $V_G - V_{th}$. As a result, the PNCs/MoS_2 phototransistor showed clear photoswitching behavior, which was superior to the case of MoS_2.

Figure 2c,d shows the responsivity and specific detectivity of the PNCs/MoS_2 and the MoS_2 phototransistors. Responsivity (R) can be obtained by the following equation $R = I_{ph}/P_{eff}$, where P_{eff} is the effective incident power which can be calculated by multiplying the optical power of the laser by the ratio of the MoS_2 channel area to the laser beam spot size. Also, based on the shot noise approximation, specific detectivity (D^*) can be obtained by the following equation $D^*_{shot} = R\sqrt{A}/\sqrt{2eI_{dark}}$, where e is the elementary charge and A is the area of a photosensitive region. As shown in Figure 2c,d, the PNCs/MoS_2 phototransistor demonstrated higher responsivity and specific detectivity compared with those of the MoS_2 phototransistor for all V_G ranges.

In Figure 2c, the responsivity of both PNCs/MoS_2 and the MoS_2 phototransistors increases at higher V_G and saturates near $V_G - V_{th}$ of ~10 V. This trend is frequently observed in photodetectors that are primarily driven by the photogating effect.[32] The photogating effect of the PNCs/MoS_2 heterostructure is attributed to the trapped holes in the PNCs and the photogating effect effectively increases the photocurrent, enabling high responsivity. On the other hand, the specific detectivity of the PNCs/MoS_2 phototransistor tends to decrease at higher gate voltages as shown in Figure 2d. This

https://doi.org/10.1021/acsnano.4c02775
ACS Nano 2024, 18, 16905−16913

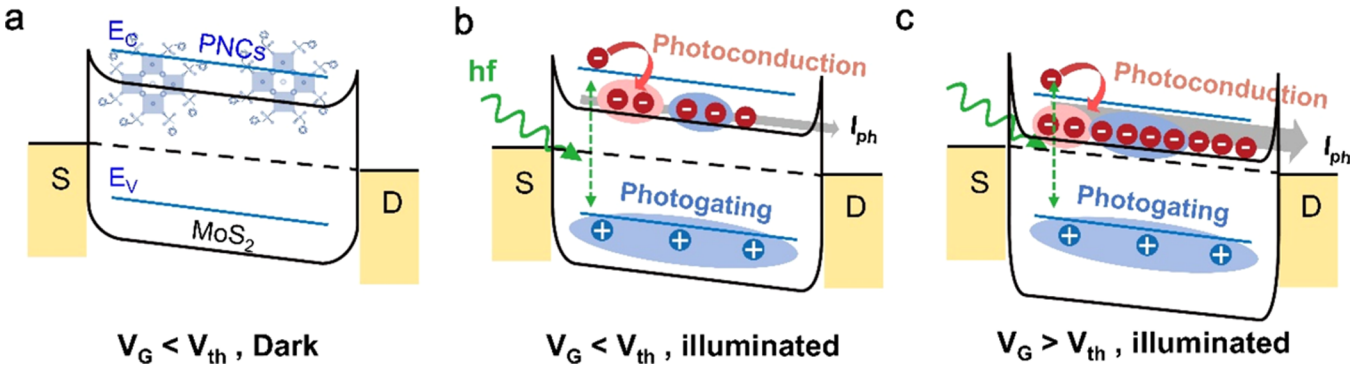

Figure 4. Band diagram illustrating the operational modes of the PNCs/MoS_2 phototransistor as a function of gate voltage and light conditions: (a) $V_G < V_{th}$, dark, (b) $V_G < V_{th}$, illuminated, and (c) $V_G > V_{th}$, illuminated.

trend is due to detectivity being defined as the responsivity divided by the square root of the dark current, which in turn increases at higher gate voltages. Note that in the case of MoS_2 phototransistors, high detectivity was observed at a very low gate voltage of −40 V, which is attributed to its much lower dark current compared to the case of PNCs/MoS_2 phototransistors.

To further analyze the photodetection performance of PNCs/MoS_2 phototransistors, contour plots depicting the responsivity and specific detectivity as functions of $V_G - V_{th}$ and incident light power are presented in Figure 2e,f. Responsivity increased with increasing V_G, while the specific detectivity tended to peak at intermediate V_G between 10 and 30 V. Furthermore, both responsivity and detectivity showed a tendency to increase as the light intensity decreased. Note that the increase in responsivity under weak light conditions is also a major indication of the photogating effect.[33] The maximum responsivity and specific detectivity within the measurement range for our phototransistors were 2.2×10^6 A/W and 9.0×10^{11} Jones respectively, which are significantly higher than previously reported values for the photodetectors utilizing similar device structures. Note that specific detectivity in Figure 2d,f is calculated based on shot noise. To calculate the accurate value of specific detectivity,[34] low-frequency noise measurements were performed (Figure S15). The comparison to the previous report is discussed in more detail in Figure 5.

The photogeneration mechanisms in photodetectors made of 2D-layered materials primarily involve photoconduction and photogating effects.[33] Photoconduction is a phenomenon in which carrier density increases by photogenerated carriers, thereby directly contributing to the increase in channel conductance. As the number of photons and carriers is proportional to the incident power, photocurrent has a linear dependence on incident power ($I_{ph} \propto P^{\alpha}$, $\alpha = 1$). On the other hand, photogating occurs when carriers generated by light become trapped at interface traps, acting as a gating source to the channel. Charge trapping on the SiO_2 surface due to water molecules[32] and spatial potential fluctuations caused by local strains between SiO_2 and 2D materials[35] are such examples of interface traps. For our device, MoS_2 and PNCs form a type II band alignment, so accumulated holes in the PNCs are the main cause of the photogating effect. In the case of photogating, the photocurrent follows a fractional power law dependence of incident power ($I_{ph} \propto P^{\alpha}$, $0 < \alpha < 1$).[36,37] If α largely varies from 1, the nonlinearity of photocurrent to the incident power is large, which indicates that photogating acts as a dominant mechanism for photocurrent generation.[11,23]

The nonlinearity of the photocurrent with respect to incident light power was calculated to observe the photogating effect at different gate voltages, as shown in Figure 3a,b. The trend lines in Figure 3a display the power law fitting $I_{ph} \propto P^{\alpha}$ for different gate voltages with the slope of the trend lines representing α. As the gate voltage increased, it was observed that α decreased from 0.70 to 0.34 and that the nonlinearity of the photocurrent dependence on incident power increased. It can be seen that α decreased as the gate voltage increased in Figure 3b. This indicates that the influence of the photogating effect contributing to the photocurrent increases as the gate voltage increases. This trend is visually confirmed in Figure 3c. Considering that photoconduction applies a constant DC offset to the photocurrent, the remaining photocurrent can be attributed to photogating. In other words, the gate dependence of the photocurrent allows us to confirm the gate dependence of the photogating effect, which is consistent with the trend observed in Figure 3b. It should be noted that the photogating effect can be interpreted as a shift of the threshold voltage, resulting in a similarity between the gate dependence of the photocurrent (Figure 3c) and the transconductance (Figure S11). Also, for reference, the value of α maintained a very low value below 0.25 across all V_G regions for MoS_2, indicating that photogating had a significant influence on MoS_2. This well agrees with the reported persistent photoconductivity phenomena of MoS_2 arising from various factors such as defects, surface adsorbates, and MoS_2/SiO_2 trap states.[38]

Another distinctive feature between photogating and photoconductive effects is the response times. Photoconduction stops generating electron−hole pairs when the light is turned off, leading to an almost immediate return to the dark current and thus to a short response time. In contrast, the photogating effect, even after the light is turned off, requires a large amount of time for the trapped charges to be detrapped before recovering to the dark current, resulting in a much longer response time.[33] Figure 3d shows the response time of the PNCs/MoS_2 phototransistor to observe the photogating effect at different gate voltages. Fall time is defined as the time it takes for I_{illum} to return to $0.1 \times I_{illum} + 0.9 \times I_{dark}$. It can be observed that the fall time increases as the gate voltage becomes higher. This also supports the fact that the influence of photogating to contribute to the photocurrent increases as the gate voltage increases. Also, it is worth mentioning that as gate voltage increases, the photocurrent increases and fall time also increases, so the optimal gate voltage condition should be determined for the specific purpose.

https://doi.org/10.1021/acsnano.4c02775
ACS Nano 2024, 18, 16905−16913

The observation can be understood through the energy band diagrams in Figure 4. Figure 4a depicts the energy band diagram of the phototransistor in the dark, with a gate voltage less than the threshold voltage ($V_G < V_{th}$). In this state, the carrier concentration within the MoS_2 channel is low. Figure 4b explains the situation when the device is illuminated with light at a gate voltage of less than the threshold voltage. The PNCs absorb the photons and generate electron−hole pairs. Electrons transfer to the MoS_2 layer and lead to an increased number of charge carriers, which is the photoconductive effect, marked in red. Concurrently, holes are confined within the PNCs, marked in blue, creating a photogating effect. Both effects synergistically contribute to the increase in the photocurrent. In Figure 4c, the condition changes such that the device is illuminated while the gate voltage is greater than the threshold voltage ($V_G > V_{th}$). Here, the channel already has an abundance of charge carriers due to the higher gate voltage. While the photogating effect is modulated by the gate voltage, the photoconductive effect remains relatively gate-independent.[36] Therefore, the photogating effect, indicated in blue, becomes more pronounced, contributing a larger proportion to the total photocurrent. Figure S12 provides a more detailed view of the gate dependence of the photogeneration mechanisms.

Figure 5 summarizes the responsivity and specific detectivity of various photodetectors based on 2D materials reported to

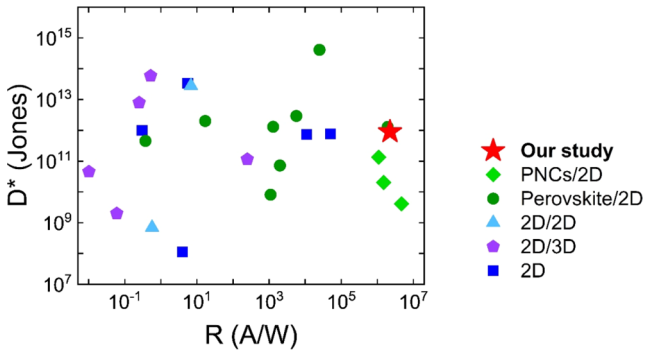

Figure 5. Photodetection performance comparison of various photodetectors based on 2D materials,[39−43] 2D/2D heterostructures,[44,45] 2D/3D heterostructures,[46−50] perovskite film/2D heterostructures,[18,19,51−56] and perovskite nanocrystals/2D heterostructures.[23]

date (Table S1 and Figure S16). Due to the extremely low dark current, 2D materials alone can exhibit high photodetection performance. However, various heterostructures have been explored to enhance its low light absorption. The 2D/2D heterostructure and perovskite film/2D heterostructure are prominent examples, but they have encountered their respective limitations and have not shown significant performance improvement compared to 2D materials. Furthermore, the PNCs/2D heterostructure utilizing 0D perovskite effectively enhanced responsivity but resulted in decreased specific detectivity due to high dark current. Unlike these heterostructures based on low-dimensional perovskite materials, in situ core/shell perovskite achieved significantly improved responsivity followed by improved specific detectivity. Since the in situ core/shell perovskite is synthesized from a thickness-controllable 3D perovskite thin film followed by an in situ splitting process, significantly increased absorbance in the active layer could be achieved by utilizing a thickness far greater than that of 2D perovskites or colloidally synthesized PNCs. Furthermore, the fast charge transport from the absence of long alkyl ligands and passivated surface trap states in core/shell structure collectively minimize carrier loss due to trap-mediated nonradiative recombination, a common issue in the extended charge transport and injection pathways toward the TMDC layer.

In future research, efforts to enhance the commercial potential of the device could be considered. First, employing MoS_2 produced via large-area film deposition, rather than mechanically exfoliated MoS_2 flakes, may facilitate broader production capabilities. Second, coating PNCs through thermal evaporation could simplify mass production. Lastly, encapsulating the PNCs could significantly improve their stability.

CONCLUSIONS

In conclusion, we have successfully developed in situ core/shell perovskite nanocrystals (PNCs)/MoS_2 heterostructure phototransistors with the aim of enhancing the photodetection performance. Through optical characterizations, we observed efficient light absorption in the PNCs layer along with efficient charge transfer from the PNCs to the MoS_2. The PNCs/MoS_2 phototransistors showed increased photocurrent compared to the MoS_2 phototransistors without PNCs. Moreover, the photodetector's responsivity and specific detectivity were also enhanced, reaching maximum values of 2.2×10^6 A/W and 9.0×10^{11} Jones, respectively. To elucidate the photocurrent generation mechanism, we systematically varied the gate voltage and the incident light power to the PNCs/MoS_2 phototransistors and observed the relationship between photocurrent and incident light power to identify two distinct phenomena of photogating and photoconductive effects. These results indicate that while photogating and photoconductive effects synergistically contribute to generating photocurrent, photogating becomes more dominant at higher gate voltages. We believe that our perovskite-MoS_2 heterostructure phototransistors demonstrate the potential of 2D material-based photodetectors, especially when they are integrated with an efficient photosensitive layer.

METHODS

MoS_2 FET Fabrication. MoS_2 flakes were mechanically exfoliated from bulk crystals and transferred to a 270 nm SiO_2/p++ Si substrate, with flake selection and thickness measurement conducted using an optical microscope and an AFM system (NX-10, Park Systems). After spin-coating of methyl methacrylate and poly(methyl methacrylate) resist layers on the MoS_2 flakes, source and drain electrodes were patterned using an electron-beam lithography system (JSM-6510, JEOL). Then, a 50 nm Au layer as electrodes was deposited using an electron-beam evaporator (KVE2004 L, Korea Vacuum Tech). The completed MoS_2 FETs were annealed at 150 °C for 1 h to enhance their electrical properties before measurement.

Integration of In Situ Core/Shell Perovskite of MoS_2 FET. To prepare the precursor solution of the mixed cation ($(FA_{0.7}MA_{0.1}GA_{0.2})_{0.87}Cs_{0.13}PbBr_3$), specific stoichiometric amounts of FABr, MABr, GABr, CsBr, and $PbBr_2$ were dissolved in dimethyl sulfoxide (DMSO) at a concentration of 0.6 M. Additionally, BPA was added at a concentration of 10 mol % relatives to $PbBr_2$. This solution was then stirred continuously overnight in a N_2-filled glovebox, ensuring thorough mixing and dissolution before its subsequent use. To synthesize in situ core/shell perovskite films, the substrate was first subjected to ultraviolet-ozone treatment to increase its hydrophilicity. The substrates were then moved to a N_2-filled glovebox. Here, metal halide perovskite (MHP) films, with a thickness of about 60 nm, were

https://doi.org/10.1021/acsnano.4c02775
ACS Nano 2024, 18, 16905−16913

formed using a spin-coating technique at 6000 rpm. This process involved the A-NCP method, where during the second stage of spinning, a solution of 2,2′,2″-benzene-1,3,5-triyltris(1-phenyl-1*H*-benzimidazole) (TPBi) in chlorobenzene (CB) was applied to the perovskite film. Following this, a solution of BPA in tetrahydrofuran (THF) was spread over the perovskite layer. The assembly was then allowed a reaction time of 15 s before being spun dry immediately afterward.

Optical and Electrical Characterization. The PL and Raman spectra were obtained through a confocal imaging system (Xper Raman 200, Nanobase) with an incident laser beam of wavelength 532 nm. The TRPL spectra were obtained through a confocal fluorescence lifetime image microscope system (FlouTime 300, PicoQuant), and the absorption spectra were obtained by using a UV−visible spectrophotometer (V-730, JASCO). The KPFM method is conducted using the AFM system (NX-10, Park Systems), and the UPS method is conducted using an X-ray photoelectron spectrometer (Versaprobe III, Ulvac-PHI). The TEM images were obtained by high-resolution transmission electron microscopy (FEI Titan 80−30 TEM, Thermo Fisher). Monolayer MoS_2 synthesized via chemical vapor deposition (CVD) was used for TRPL and UV−visible spectroscopy. The electrical characteristics of FETs were measured by using a probe station (M6VC, MSTECH) and a semiconductor parameter analyzer (Keithley 4200). The photoresponses of FETs were measured under laser (MDE5240 V) illumination of wavelength 520 nm. The laser beam was globally illuminated to phototransistors with a few millimeters in diameter. All of the characterizations were performed at room temperature. To minimize unwanted ambient air exposure, PNCs/MoS_2 phototransistors were moved from an N_2-filled glovebox to characterization equipment using metal containers. These containers are designed to keep a vacuum inside and shield the devices from external degrading factors such as humidity, various gases in the environment, and light exposure.

ASSOCIATED CONTENT

Supporting Information

The Supporting Information is available free of charge at https://pubs.acs.org/doi/10.1021/acsnano.4c02775.

Additional details on device fabrication process, thickness and optical characterization of in situ core/shell perovskite, MoS_2, PL lifetime of PNCs/MoS_2 heterostructure with different thickness, KPFM and UPS characterization of PNCs/MoS_2 heterostructure for calculating the energy band alignments, electrical characterization of PNCs and MoS_2 FET, dynamic photoswitching behavior of MoS_2 FET, detailed explanation of photogating and photoconductive effect on PNCs/MoS_2 phototransistors, stability and noise of PNCs/MoS_2 phototransistors, and comparison of photodetection figure of merits with other reports (PDF)

AUTHOR INFORMATION

Corresponding Authors

Tae-Woo Lee − *Department of Materials Science and Engineering, Research Institute of Advanced Materials, and Institute of Engineering Research, Seoul National University, Seoul 08826, Korea; SN DISPLAY Co., Ltd., Seoul 08826, Korea;* orcid.org/0000-0002-6449-6725; Email: twlees@snu.ac.kr

Kyungjune Cho − *Convergence Research Center for Solutions to Electromagnetic Interference in Future-mobility, Korea Institute of Science and Technology, Seoul 02792, Korea;* Email: kcho@kist.re.kr

Keehoon Kang − *Department of Materials Science and Engineering, Research Institute of Advanced Materials, and Institute of Applied Physics, Seoul National University, Seoul 08826, Korea;* orcid.org/0000-0003-1230-3626; Email: keehoon.kang@snu.ac.kr

Takhee Lee − *Department of Physics and Astronomy, Seoul National University, Seoul 08826, Korea; Institute of Applied Physics, Seoul National University, Seoul 08826, Korea;* orcid.org/0000-0001-5988-5219; Email: tlee@snu.ac.kr

Authors

Jinwoo Sim − *Department of Physics and Astronomy, Seoul National University, Seoul 08826, Korea*

Sunggyu Ryoo − *Department of Physics and Astronomy, Seoul National University, Seoul 08826, Korea*

Joo Sung Kim − *Department of Materials Science and Engineering, Seoul National University, Seoul 08826, Korea; SN DISPLAY Co., Ltd., Seoul 08826, Korea*

Juntae Jang − *Department of Physics and Astronomy, Seoul National University, Seoul 08826, Korea*

Heebeom Ahn − *Department of Materials Science and Engineering, Seoul National University, Seoul 08826, Korea*

Donguk Kim − *Department of Physics and Astronomy, Seoul National University, Seoul 08826, Korea*

Joonha Jung − *Department of Materials Science and Engineering, Seoul National University, Seoul 08826, Korea*

Taehyun Kong − *Department of Materials Science and Engineering, Seoul National University, Seoul 08826, Korea*

Hyeonmin Choi − *Department of Materials Science and Engineering, Seoul National University, Seoul 08826, Korea*

Yun Seog Lee − *Department of Mechanical Engineering, Seoul National University, Seoul 08826, Korea;* orcid.org/0000-0002-2289-109X

Complete contact information is available at: https://pubs.acs.org/10.1021/acsnano.4c02775

Author Contributions

◆J.S., S.R., and J.S.K. contributed equally to this work.

Notes

The authors declare no competing financial interest.

ACKNOWLEDGMENTS

The authors appreciate the financial support of the National Research Foundation of Korea (NRF) grant (No. 2021R1A2C3004783, No. RS-2024-00342191, and No. 2021R1C1C2091728), the BrainLink program (No. 2022H1D3A3A01077343), and the Nano•Material Technology Development Program grant (No. 2021M3H4A1A02049651) through NRF funded by the Ministry of Science and ICT of Korea, and the industry−university cooperation program by Samsung Electronics Co., Ltd. (IO201211-08047-01). J.S.K. and T.-W.L. acknowledge the NRF grant BrainLink program (2022H1D3A3A01081288). K.C. acknowledges the National Research Council of Science & Technology (NST) grant (CRC22031-000). J.S. and S.R. acknowledge support from the Student Directed Education (Undergraduate Research) Program at the Faculty of Liberal Education, Seoul National University (2023). This work was also supported by the Research Grant from Seoul National University (0417-20230167).

REFERENCES

(1) Wang, Q. H.; Kalantar-Zadeh, K.; Kis, A.; Coleman, J. N.; Strano, M. S. Electronics and Optoelectronics of Two-Dimensional

Transition Metal Dichalcogenides. *Nat. Nanotechnol.* **2012**, *7*, 699–712.
(2) Manzeli, S.; Ovchinnikov, D.; Pasquier, D.; Yazyev, O. V.; Kis, A. 2D Transition Metal Dichalcogenides. *Nat. Rev. Mater.* **2017**, *2*, No. 17033.
(3) Radisavljevic, B.; Radenovic, A.; Brivio, J.; Giacometti, V.; Kis, A. Single-Layer MoS_2 Transistors. *Nat. Nanotechnol.* **2011**, *6*, 147–150.
(4) Kim, H.; Uddin, S. Z.; Higashitarumizu, N.; Rabani, E.; Javey, A. Inhibited Nonradiative Decay at All Exciton Densities in Monolayer Semiconductors. *Science* **2021**, *373*, 448–452.
(5) Jiang, J.; Wen, Y.; Wang, H.; Yin, L.; Cheng, R.; Liu, C.; Fang, L.; He, J. Recent Advances in 2D Materials for Photodetectors. *Adv. Electron. Mater.* **2015**, *7*, No. 2001125.
(6) Cheng, Y.; Wan, R.; Li, L.; Liu, Z.; Yan, S.; Li, L.; Wang, J.; Gao, Y. Research Progress on Improving the Performance of MoS_2 Photodetector. *J. Opt.* **2022**, *24*, No. 104003.
(7) Lopez-Sanchez, O.; Lembke, D.; Kayci, M.; Radenovic, A.; Kis, A. Ultrasensitive Photodetectors Based on Monolayer MoS_2. *Nat. Nanotechnol.* **2013**, *8*, 497–501.
(8) Seo, W.; Park, W.; Seo, H. Y.; Oh, S.; Kwon, O.; Jeong, S. H.; Kim, D. H.; Kim, M. J.; Lee, S. K.; Lee, B. H.; Cho, B. MoS_2/p-Si Heterojunction with Graphene Interfacial Layer for High Performance 940 nm Infrared Photodetector. *Appl. Surf. Sci.* **2022**, *604*, No. 154485.
(9) Kuo, L.; Sangwan, V. K.; Rangnekar, S. V.; Chu, T.; Lam, D.; Zhu, Z.; Richter, L. J.; Li, R.; Szydłowska, B. M.; Downing, J. R.; Luijten, B. J.; Lauhon, L. J.; Hersam, M. C. All-printed Ultrahigh-responsivity MoS_2 Nanosheet Photodetectors Enabled by Megasonic Exfoliation. *Adv. Mater.* **2022**, *34*, No. 2203772.
(10) Zhang, W.; Chiu, M.-H.; Chen, C.-H.; Chen, W.; Li, L.-J.; Wee, A. T. Role of Metal Contacts in High-Performance Phototransistors Based on WSe_2 Monolayers. *ACS Nano* **2014**, *8*, 8653–8661.
(11) Wu, H.; Si, H.; Zhang, Z.; Kang, Z.; Wu, P.; Zhou, L.; Zhang, S.; Zhang, Z.; Liao, Q.; Zhang, Y. All-Inorganic Perovskite Quantum Dot-Monolayer MoS_2 Mixed-Dimensional Van der Waals Heterostructure for Ultrasensitive Photodetector. *Adv. Sci.* **2018**, *5*, No. 1801219.
(12) Seo, D.; Lee, D. Y.; Kwon, J.; Lee, J. J.; Taniguchi, T.; Watanabe, K.; Lee, G.-H.; Kim, K. S.; Hone, J.; Kim, Y. D.; Choi, H. J. High-Performance Monolayer MoS_2 Field-Effect Transistor with Large-Scale Nitrogen-Doped Graphene Electrodes for Ohmic Contact. *Appl. Phys. Lett.* **2019**, *115*, No. 012104.
(13) Kozawa, D.; Pu, J.; Shimizu, R.; Kimura, S.; Chiu, M.-H.; Matsuki, K.; Wada, Y.; Sakanoue, T.; Iwasa, Y.; Li, L.-J.; Takenobu, T. Photodetection in p-n Junctions Formed by Electrolyte-Gated Transistors of Two-Dimensional Crystals. *Appl. Phys. Lett.* **2016**, *109*, No. 201107.
(14) Gao, A.; Liu, E.; Long, M.; Zhou, W.; Wang, Y.; Xia, T.; Hu, W.; Wang, B.; Miao, F. Gate-Tunable Rectification Inversion and Photovoltaic Detection in Graphene/WSe_2 Heterostructures. *Appl. Phys. Lett.* **2016**, *108*, No. 223501.
(15) Zhou, X.; Hu, X.; Zhou, S.; Song, H.; Zhang, Q.; Pi, L.; Li, L.; Li, H.; Lü, J.; Zhai, T. Tunneling Diode Based on WSe_2/SnS_2 Heterostructure Incorporating High Detectivity and Responsivity. *Adv. Mater.* **2018**, *30*, No. 1703286.
(16) Yu, W.; Li, S.; Zhang, Y.; Ma, W.; Sun, T.; Yuan, J.; Fu, K.; Bao, Q. Near-Infrared Photodetectors Based on $MoTe_2$/Graphene Heterostructure with High Responsivity and Flexibility. *Small* **2017**, *13*, No. 1700268.
(17) Mudd, G. W.; Svatek, S. A.; Hague, L.; Makarovsky, O.; Kudrynskyi, Z. R.; Mellor, C. J.; Beton, P. H.; Eaves, L.; Novoselov, K. S.; Kovalyuk, Z. D.; Vdovin, E. E.; Marsden, A. J.; Wilson, N. R.; Patanè, A. High Broad-Band Photoresponsivity of Mechanically Formed InSe-Graphene van der Waals Heterostructures. *Adv. Mater.* **2015**, *27*, 3760–3766.
(18) Kang, D.-H.; Pae, S. R.; Shim, J.; Yoo, G.; Jeon, J.; Leem, J. W.; Yu, J. S.; Lee, S.; Shin, B.; Park, J.-H. An Ultrahigh-Performance Photodetector based on a Perovskite-Transition-Metal-Dichalcogenide Hybrid Structure. *Adv. Mater.* **2016**, *28*, 7799–7806.
(19) Wen, W.; Zhang, W.; Wang, X.; Feng, Q.; Liu, Z.; Yu, T. Ultrasensitive Photodetectors Promoted by Interfacial Charge Transfer from Layered Perovskites to Chemical Vapor Deposition-Grown MoS_2. *Small* **2021**, *17*, No. 2102461.
(20) Wang, H.; Wang, X.; Chen, Y.; Zhang, S.; Jiang, W.; Zhang, X.; Qin, J.; Wang, J.; Li, X.; Pan, Y.; et al. Extremely Low Dark Current MoS_2 Photodetector via 2D Halide Perovskite as the Electron Reservoir. *Adv. Opt. Mater.* **2020**, *8*, No. 1901402.
(21) Manser, J. S.; Christians, J. A.; Kamat, P. V. Intriguing Optoelectronic Properties of Metal Halide Perovskites. *Chem. Rev.* **2016**, *116*, 12956–13008.
(22) Song, X.; Liu, X.; Yu, D.; Huo, C.; Ji, J.; Li, X.; Zhang, S.; Zou, Y.; Zhu, G.; Wang, Y.; Wu, M.; Xie, A.; Zeng, H. Boosting Two-Dimensional MoS_2/$CsPbBr_3$ Photodetectors via Enhanced Light Absorbance and Interfacial Carrier Separation. *ACS Appl. Mater. Interfaces* **2018**, *10*, 2801–2809.
(23) Jeong, S.-J.; Cho, S.; Moon, B.; Teku, J. A.; Jeong, M.-H.; Lee, S.; Kim, Y.; Lee, J.-S. Zero Dimensional-Two Dimensional Hybrid Photodetectors Using Multilayer MoS_2 and Lead Halide Perovskite Quantum Dots with a Tunable Bandgap. *ACS Appl. Mater. Interfaces* **2023**, *15*, 5432–5438.
(24) Kim, J. S.; Heo, J.-M.; Park, G.-S.; Woo, S.-J.; Cho, C.; Yun, H. Y.; Kim, D.-H.; Park, J.; Lee, S.-C.; Park, S.-H.; Yoon, E.; Greenham, N. C.; Lee, T.-W. Ultra-Bright, Efficient and Stable Perovskite Light-Emitting Diodes. *Nature* **2022**, *611*, 688–694.
(25) Giovanni, D.; Righetto, M.; Zhang, Q.; Lim, J. W.; Ramesh, S.; Sum, T. C. Origins of the Long-Range Exciton Diffusion in Perovskite Nanocrystal Films: Photon Recycling vs. Exciton Hopping. *Light: Sci. Appl.* **2021**, *10*, No. 2.
(26) Splendiani, A.; Sun, L.; Zhang, Y.; Li, T.; Kim, J.; Chim, C.-Y.; Galli, G.; Wang, F. Emerging Photoluminescence in Monolayer MoS_2. *Nano Lett.* **2010**, *10*, 1271–1275.
(27) Khatua, D. P.; Singh, A.; Gurung, S.; Tanwa, M.; Kumar, R.; Jayabalan, J. A Comparative Study of Ultrafast Carrier Dynamics Near A, B, and C-Excitons in a Monolayer MoS_2 at High Excitation Densities. *Opt. Mater.* **2022**, *126*, No. 112224.
(28) Sturman, B.; Podivilov, E.; Gorkunov, M. Origin of Stretched Exponential Relaxation for Hopping-Transport Models. *Phys. Rev. Lett.* **2003**, *91*, No. 176602.
(29) Bartel, T.; Dworzak, M.; Strassburg, M.; Hoffmann, A.; Strittmatter, A.; Bimberg, D. Recombination Dynamics of Localized Excitons in InGaN Quantum Dots. *Appl. Phys. Lett.* **2004**, *85*, 1946–1948.
(30) Chen, Y.; Wang, Y.; Wang, Z.; Gu, Y.; Ye, Y.; Chai, X.; Ye, J.; Chen, Y.; Xie, R.; Zhou, Y.; Hu, Z.; Li, Q.; Zhang, L.; Wang, F.; Wang, P.; Miao, J.; Wang, J.; Chen, X.; Lu, W.; Zhou, P.; Hu, W. Unipolar Barrier Photodetectors Based on van der Waals Heterostructures. *Nat. Electron.* **2021**, *4*, 357–363.
(31) Chen, J.-S.; Li, M.; Wu, Q.; Fron, E.; Tong, X.; Cotlet, M. Layer-Dependent Photoinduced Electron Transfer in 0D-2D Lead Sulfide/Cadmium Sulfide-Layered Molybdenum Disulfide Hybrids. *ACS Nano* **2019**, *13*, 8461–8468.
(32) Furchi, M. M.; Polyushkin, D. K.; Pospischil, A.; Mueller, T. Mechanisms of Photoconductivity in Atomically Thin MoS_2. *Nano Lett.* **2014**, *14*, 6165–6170.
(33) Fang, H.; Hu, W. Photogating in Low Dimensional Photodetectors. *Adv. Sci.* **2017**, *4*, No. 1700323.
(34) Wang, F.; Zhang, T.; Xie, R.; Wang, Z.; Hu, W. How to Characterize Figures of Merit of Two-Dimensional Photodetectors. *Nat. Commun.* **2023**, *14*, No. 2224.
(35) Chen, P.-H.; Chen, C.-A.; Lin, Y.-T.; Hsieh, P.-Y.; Chuang, M.-H.; Liu, X.; Hsieh, T.-Y.; Shen, C.-H.; Shieh, J.-M.; Wu, M.-C.; Chen, Y.-F.; Yang, C.-C.; Lee, Y.-H. Passivated Interfacial Traps of Monolayer MoS_2 with Bipolar Electrical Pulse. *ACS Appl. Mater. Interfaces* **2023**, *15* (8), 10812–10819.
(36) Island, J. O.; Blanter, S. I.; Buscema, M.; van der Zant, H. S. J.; Castellanos-Gomez, A. Gate Controlled Photocurrent Generation Mechanisms in High-Gain In_2Se_3 Phototransistors. *Nano Lett.* **2015**, *15*, 7853–7858.

https://doi.org/10.1021/acsnano.4c02775
ACS Nano 2024, 18, 16905–16913

(37) Zhang, W.; Huang, J.; Chen, C.; Chang, Y.; Cheng, Y.; Li, L. High-Gain Phototransistors Based on a CVD MoS_2 Monolayer. *Adv. Mater.* **2013**, *25*, 3456−3461.
(38) Cho, K.; Kim, T.-Y.; Park, W.; Park, J.; Kim, D.; Jang, J.; Jeong, H.; Hong, S.; Lee, T. Gate-Bias Stress-Dependent Photoconductive Characteristics of Multi-Layer MoS_2 Field Effect Transistors. *Nanotechnology* **2014**, *25*, No. 155201.
(39) Kufer, D.; Konstantatos, G. Highly Sensitive, Encapsulated MoS_2 Photodetector with Gate Controllable Gain and Speed. *Nano Lett.* **2015**, *15* (11), 7307−7313.
(40) Wu, D.; Guo, C.; Zeng, L.; Ren, X.; Shi, Z.; Wen, L.; Chen, Q.; Zhang, M.; Li, X. J.; Shan, C.-X.; Jie, J. Phase-Controlled van der Waals Growth of Wafer-Scale 2D $MoTe_2$ Layers for Integrated High-Sensitivity Broadband Infrared Photodetection. *Light Sci. Appl.* **2023**, *12*, No. 5, DOI: 10.1038/s41377-022-01047-5.
(41) Ye, P.; Xiao, H.; Zhu, Q.; Kong, Y.; Tang, Y.; Xu, M. Si-CMOS-Compatible 2D $PtSe_2$-Based Self-Driven Photodetector with Ultrahigh Responsivity and Specific Detectivity. *Sci. China Mater.* **2023**, *66*, 193−201.
(42) Yin, J.; Liu, L.; Zang, Y.; Ying, A.; Hui, W.; Jiang, S.; Zhang, C.; Yang, T.; Chueh, Y.-L.; Li, J.; Kang, J. Engineered Tunneling Layer with Enhanced Impact Ionization for Detection Improvement in Graphene/Silicon Heterojunction Photodetectors. *Light Sci. Appl.* **2021**, *10*, No. 113, DOI: 10.1038/s41377-021-00553-2.
(43) Yang, Y.; Jeon, J.; Park, J.-H.; Jeong, M. S.; Lee, B. H.; Hwang, E.; Lee, S. Plasmonic Transition Metal Carbide Electrodes for High-Performance InSe Photodetectors. *ACS Nano* **2019**, *13* (8), 8804−8810.
(44) Ahn, J.; Ko, K.; Kyhm, J.-h.; Ra, H.-S.; Bae, H.; Hong, S.; Kim, D.-Y.; Jang, J.; Kim, T. W.; Choi, S.; Kang, J.-H.; Kwon, N.; Park, S.; Ju, B.-K.; Poon, T.-C.; Park, M.-C.; Im, S.; Hwang, D. K. Near-Infrared Self-Powered Linearly Polarized Photodetection and Digital Incoherent Holography Using $WSe_2/ReSe_2$ van der Waals Heterostructure. *ACS Nano* **2021**, *15* (11), 17917−17925.
(45) Ning, J.; Zhou, Y.; Zhang, J.; Lu, W.; Dong, J.; Yan, C.; Wang, D.; Shen, X.; Feng, X.; Zhou, H.; Hao, Y. Self-Driven Photodetector Based on a GaSe/$MoSe_2$ Selenide van der Waals Heterojunction with the Hybrid Contact. *Appl. Phys. Lett.* **2020**, *117* (16), No. 163104.
(46) Choi, J.-M.; Jang, H. Y.; Kim, A. R.; Kwon, J.-D.; Cho, B.; Park, M. H.; Kim, Y. Ultra-Flexible and Rollable 2D-MoS_2/Si Heterojunction-Based Near-Infrared Photodetector via Direct Synthesis. *Nanoscale* **2021**, *13*, 672−680.
(47) Wu, D.; Guo, C.; Wang, Z.; Ren, X.; Tian, Y.; Shi, Z.; Lin, P.; Tian, Y.; Chen, Y.; Li, X. A Defect-Induced Broadband Photodetector Based on WS_2/Pyramid Si 2D/3D Mixed-Dimensional Heterojunction with a Light Confinement Effect. *Nanoscale* **2021**, *13*, 13550−13557.
(48) Shen, J.; Liu, X.; Song, X.; Li, X.; Wang, J.; Zhou, Q.; Luo, S.; Feng, W.; Wei, X.; Lu, S.; Feng, S.; Du, C.; Wang, Y.; Shi, H.; Wei, D. High-Performance Schottky Heterojunction Photodetector with Directly Grown Graphene Nanowalls as Electrodes. *Nanoscale* **2017**, *9*, 6020−6025.
(49) Lu, J.; Zhang, L.; Ma, C.; Huang, W.; Ye, Q.; Yi, H.; Zheng, Z.; Yang, G.; Liu, C.; Yao, J. In Situ Integration of Te/Si 2D/3D Heterojunction Photodetectors Toward UV−vis−IR Ultra-Broadband Photoelectric Technologies. *Nanoscale* **2022**, *14*, 6228−6238.
(50) Wu, D.; Xu, M.; Zeng, L.; Shi, Z.; Tian, Y.; Li, X. J.; Shan, C.-X.; Jie, J. In Situ Fabrication of $PdSe_2$/GaN Schottky Junction for Polarization-Sensitive Ultraviolet Photodetection with High Dichroic Ratio. *ACS Nano* **2022**, *16* (4), 5545−5555.
(51) Fang, C.; Wang, H.; Shen, Z.; Shen, H.; Wang, S.; Ma, J.; Wang, J.; Luo, H.; Li, D. High-Performance Photodetectors Based on Lead-Free 2D Ruddlesden−Popper Perovskite/MoS_2 Heterostructures. *ACS Appl. Mater. Interfaces* **2019**, *11* (8), 8419−8427.
(52) Wang, L.; Zou, X.; Lin, J.; Jiang, J.; Liu, Y.; Liu, X.; Zhao, X.; Liu, Y. F.; Ho, J. C.; Liao, L. Perovskite/Black Phosphorus/MoS_2 Photogate Reversed Photodiodes with Ultrahigh Light On/Off Ratio and Fast Response. *ACS Nano* **2019**, *13* (4), 4804−4813.
(53) Ma, C.; Shi, Y.; Hu, W.; Chiu, M.-H.; Liu, Z.; Bera, A.; Li, F.; Wang, H.; Li, L.-J.; Wu, T. Heterostructured $WS_2/CH_3NH_3PbI_3$ Photoconductors with Suppressed Dark Current and Enhanced Photodetectivity. *Adv. Mater.* **2016**, *28*, 3683−3689.
(54) Zhang, Z.-X.; Zeng, L.-H.; Tong, X.-W.; Gao, Y.; Xie, C.; Tsang, Y. H.; Luo, L.-B.; Wu, Y.-C. Ultrafast, Self-Driven, and Air-Stable Photodetectors Based on Multilayer $PtSe_2$/Perovskite Heterojunctions. *J. Phys. Chem. Lett.* **2018**, *9* (6), 1185−1194.
(55) Li, J.; Yuan, S.; Tang, G.; Li, G.; Liu, D.; Li, J.; Hu, X.; Liu, Y.; Li, J.; Yang, Z.; Liu, S. F.; Liu, Z.; Gao, F.; Yan, F. High-Performance, Self-Powered Photodetectors Based on Perovskite and Graphene. *ACS Appl. Mater. Interfaces* **2017**, *9* (49), 42779−42787.
(56) Zhou, D.; Yu, L.; Zhu, P.; Zhao, H.; Feng, S.; Shen, J. Lateral Structured Phototransistor Based on Mesoscopic Graphene/Perovskite Heterojunctions. *Nanomaterials* **2021**, *11* (3), 641.

https://doi.org/10.1021/acsnano.4c02775
ACS Nano 2024, 18, 16905−16913